JOURNAL OF BUILDING PERFORMANCE SIMULATION
2025, VOL. 18, NO. 2, 229–246
https://doi.org/10.1080/19401493.2024.2432915

LiDICS: a light dynamics interface for multi-domain simulation based on the FMI-standard

Simon O. Weber[a], Yuan Fang[b], Daniel Rüdisser[c] and Philip Leistner[a,b]

[a]Institute for Acoustics and Building Physics, University of Stuttgart, Stuttgart, Germany; [b]Fraunhofer Institute for Building Physics, Stuttgart, Germany; [c]HTflux Engineering GmbH, Graz, Austria

ABSTRACT
The assessment of adaptive façades faces several challenges, including the representation of adjustable material and geometric properties within building performance simulation. This paper introduces a methodical and model-based interface dedicated to this issue. Adjustable material and geometric façade properties can be captured and continuously adapted within the building performance simulation using this model, without the need to reinitialise the simulation as required with matrix-based methods. The method comprises two steps: model training and export. Model training transforms ray-tracing-based sampling outcomes into an algebraic function. Model export generates a Functional Mock-up Unit. The LiDICS method is applied to switchable membrane cushion constructions with complementary printing patterns. The model training achieves a high accuracy ($r^2 = 99.4\%$). Subsequently, an inter-model validation is conducted using annual simulation from the RADIANCE 3-phase method, likewise resulting in high accuracy ($r^2 = 98.5\%$). Lastly, a brief analysis is conducted to compare four operation strategies regarding coupled comfort and energy assessment.

ARTICLE HISTORY
Received 25 March 2024
Accepted 16 November 2024

KEYWORDS
Complex fenestration; adaptive façades; multi domain simulation; spherical harmonics; incidence operator regularization; functional mock-up interface

1. Introduction

The United Nations recently published 2021 Global Status Report for Buildings and Construction indicates that the building sector is responsible for 37% of global carbon dioxide emissions and 36% of global energy use (UNEP 2021). The Collaborative Research Centre 1244 at the University of Stuttgart is intensively addressing the reduction of the buildings carbon emission through mass reduction and adaptability. As part of this work, the world's first adaptive high-rise experimental building D1244 (Blandini et al. 2022) was built. In addition to adaptive truss structures, adaptive façades represent the second research focus. They have the potential to reduce carbon emissions while increasing occupant comfort. This potential lies in the façades material and geometric properties that can be adjusted to changing indoor and outdoor environmental conditions.

This work utilizes switchable membrane cushion constructions as an application object for adaptive façades. Membrane cushions offer significant potential for carbon emission reduction due to their light weight induced reduction in load-bearing structure, excellent recyclability and other sustainable attributes. Customisable, switchable shading effects can be achieved by incorporating complementary printed patterns. In this context, 'complementary' signifies that when the printed layers are adjacent to each other, no direct light can pass through. However, when the spaces between the layers are inflated, light is able to pass through the structure at an angle, cf. Figure 7.

The spacing between the membrane layers represents the adjustable geometric properties of the façade, refered to as the 'façade input'. Adjusting these façade inputs affects daylight-related metrics such as mean workplace illuminance, useful daylight illuminance, and daylight glare probability. Furthermore, thermal variables are also influenced, including the U-value and solar heat gain coefficient, that are crucial for thermal comfort and energy efficiency.

Underlying these interactions are light-related properties, referred to as the 'quantities'. For membrane cushion constructions, these include illuminance levels measured by sensors at the workplace and at eye level, as well as solar absorptions within individual layers and transmission through the cushion structure. In this work, the term 'complex light dynamic' signifies an algebraic relationship between a quantity, a one- or multi-dimensional façade input and sun or sky specific influences. The prefix 'complex' refers to a strong dependence on the sun angles.

CONTACT Simon O. Weber simon.weber@iabp.uni-stuttgart.de

Overall, switchable membrane cushion constructions are emblematic of many adaptive façades. Their assessment involves complex light dynamics and interactions within the thermal, solar-thermal and daylight domains. However, there are many obstacles in the assessment of adaptive façades.

What are the challenges in the assessment of adaptive façade variants?

Numerous challenges confront the performance prediction of adaptive façades (Loonen et al. 2017; Taveres-Cachat et al. 2021).

Firstly, there's a necessity to model adjustable material and geometric façade properties, which current building performance simulation tools struggle with (Loonen et al. 2017; Taveres-Cachat et al. 2021). While workarounds have been devised, they introduce further issues (Borkowski, Rovas, and Raslan 2021; Favoino et al. 2018; Loonen et al. 2017). Loonen et al. (2017) suggest employing the Modelica language for its flexibility in creating customized models, such as defining the thickness of thermal resistance in the resistance-capacitance network of a membrane façade as a time-variant model input.

Secondly, adaptive façades exhibit pronounced angular dependency in their properties concerning visual and solar light effects. Daylight behaviour is modelled as angle-dependent by default, e.g. using the matrix based methods. This is not always the case for the energetic light component. The non-angle-dependent modelling of the solar heat gain coefficient can lead to large deviations in the forecast of the annual energy demand and the design capacities of heating and cooling (Weber et al. 2023b). Therefore, 'it is very important to use the correct angular dependence in building simulations' (Kuhn et al. 2011).

A third challenge for performance prediction arises from the 'strong mutual dependence between design and control aspects' (Loonen et al. 2017). This has dual implications.

Firstly, to assess design variants from a life cycle perspective, façade control must be comparative, encompassing all system states while meeting energy efficiency and multi domain comfort constraints. With mutual dependence in multiple domains, 'there may be a need to solve the differential equations that describe the relevant physical phenomena in a coupled way' (Loonen et al. 2017). The concept of 'model predictive control is, in theory, ideal to ensure the most significant improvement in the operation of advanced building envelopes' (Taveres-Cachat et al. 2021) but require twice continuous differentiable algebraic model equations.

Secondly, in the life cycle assessment of adaptive façades, high-tech components typically exhibit shorter lifecycles, while active control increases wear, leading to increased manufacturing and maintenance costs (Crespi and Persiani 2019). Dynamic simulations, coupled with a control concept, are essential to estimating and integrating wear into life cycle assessment, ensuring a reduction in life cycle costs by compensating for increased efforts through potential reductions in the operating phase B6.

How do others model, couple and control adaptive façades?

According to the review (Taveres-Cachat et al. 2021), the coupling of domain-specific simulation models is distinguished based on coupling variables, strategies, techniques, and frequencies. An even more comprehensive differentiation is proposed in the present work, cf. Table A1. The system model, depicted in Figure 1, was utilized to classify the literature work. Within it, the model 'CLDM' is subdivided into the visual and solar domain. Within the model 'Daylight', metrics like useful daylight illuminance or simplified daylight glare probability are derived from illuminance values. In the model 'Thermal', the commonly employed resistance network of the façade is linked to solar heat sources and the transient room model. The prerequisite for inclusion in the literature review is the combination of modelling at least one light domain with an operation strategy.

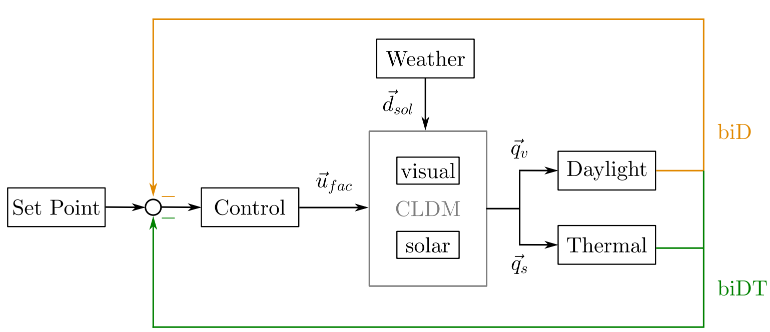

Figure 1. System dynamics scheme with complex light dynamics model (CLDM).

The literature review shows that either the tint state, a rotation angle, an overhang height or a gap width is considered as the façade input type.

All studies analyzed employ a sequential coupling strategy between ray tracing and dynamic simulation. The CLDM models are precalculated sequentially for discrete façade input values and then coupled to the total system. Conversely, bidirectional coupling of dynamic control and a ray tracing tool, although theoretically conceivable, is not practically implemented perhaps due to the considerable computational demand.

Matrix based methods, primarily the 3-phase method, are universally utilized across all studies as the reduction technique for the visual light model. View, transmission, and daylight matrices are determined using the RADIANCE tool (Ward 1994). The reduction method for the solar light model encompasses either 3-phase method with RADIANCE, the Klems matrix layer method (Klems 1993) within WINDOW (Curcija et al. 2018), or the Kuhn method (Kuhn et al. 2011).

Regarding dynamic control, the quantity corresponding to the applied continuous façade input must be queried from the precalculated discrete values. While some studies utilize interpolation methods to obtain continuous quantities, most rely on discrete query. If control is conducted as usually through the solution of a heuristic, an integer program (Coffey et al. 2022), or a mixed integer program (Gehbauer, Lee, and Wang 2023), no continuous query and interpolation is needed. This simplifies the effort for multidimensional problems. Nevertheless, depending on the façade type, a discrete selection of façade states could potentially compromise energy efficiency and multi domain comfort. Moreover, a higher resolution of discretisation would amplify the complexity of the heuristics or integer optimization. In the context of control being conducted through non-linear programming, such as in model predictive control, twice continuous differentiability becomes a prerequisite and thus continuous query and interpolation.

The number of independent façade inputs typically remains one. In cases where the dimension exceeds one, it is consistently represented through partitioning of a façade area into parallel and individually controllable window regions. There has not been an instance where a region was modelled with a multivariate façade input. However, such a scenario would arise with a basic blind, for instance, if it were modelled using both the angle of rotation and the height of the slats.

With multidimensional façade inputs, the potential combinations between all discrete points of each input proliferate rapidly. Consequently, identifying the appropriate combination of the multidimensional façade input by the control system becomes progressively intricate. To mitigate this complexity, several studies have employed an area based superposition methodology, as illustrated in Figure 2. This methodology reduces the dependency of the quantity to a superposition of several one-dimensional single input single output models. Shen and Han (2022) term this approach as the individual daylight contribution, which signifies a substantial reduction in complexity. However, it is deemed erroneous since light is either reflected or transmitted by other window elements depending on their façade inputs. An attempt to circumvent this issue is made by assuming low reflections from the other façade regions (Shen and Han 2022). Similarly, no reflection ($I'_n(\lambda) = 0$) of the transmitted energetic light components is assumed within the ISO 52022-3 calculation of the solar heat gain coefficient.

The integration of complex light models into dynamic simulations typically follows a one-to-one coupling approach. For instance, in the study (de Vries, Loonen, and Hensen 2021), the quantity is transmitted to the control model through table lookups in MATLAB. This stands in contrast to the approach adopted in this publication, where the CLDM model is integrated into the system model via standard-interface coupling.

Concerning control development 'most building performance simulation tools (…) offer only limited means to describe more complex control behaviour' (de Vries, Loonen, and Hensen 2021). The primary control method employed is threshold based heuristic control, predominantly reliant on bidirectional daylight states of the

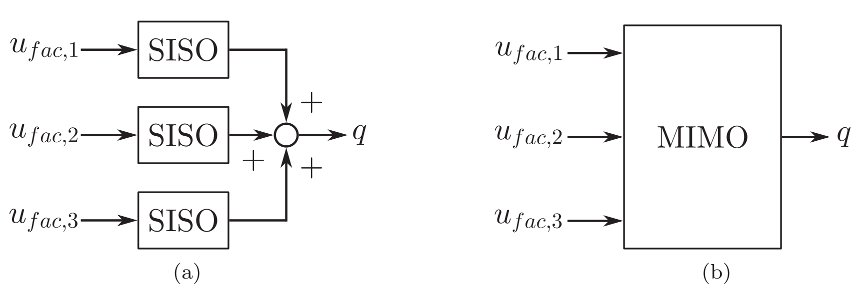

Figure 2. Complexity reduction methods for high-dimensional façade input $\vec{u}_{fac}$. (a) Applied superposition method. (b) Applied MISO model.

system model. In instances where optimization based control methods were utilized, daylight and thermal states were frequently incorporated into the control of the system.

Why do we need LiDICS?

LiDICS, from **Li**ght **D**ynamics **I**nterface for **C**oupled **S**imulation, is a methodical workflow step within the proposed assessment workflow of adaptive façades, cf. Figure 3. However, LiDICS is not merely a methodical but also a model based interface. Like any interface, it serves as a connection between two points and enables the exchange of data and information. The LiDICS method is positioned between domain-specific sampling, predominantly ray tracing based, and the multi-domain simulation and assessment of the adaptive façades. The LiDICS modelling interface presupposes the system dynamics scheme, cf. Figure 4, with façade inputs $\vec{u}_{fac}$ and weather-dependent solar disturbances $\vec{d}_{sol}$, as well as quantity outputs $\vec{q}$.

The LiDICS method transforms sampling outcomes into a twice continuously differentiable algebraic model. In doing so, it addresses the presented assessment challenges: the representation of adjustable material and geometric properties and the strong angle-dependency. The property of twice continuous differentiability creates a prerequisite for developing optimal control concepts. These concepts subsequently enable the simultaneous consideration of mutual influences on multi-domain

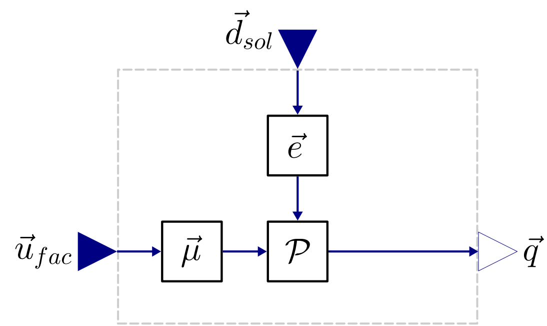

Figure 4. System dynamics scheme of the CLDM Modelica model for model export.

comfort and energy efficiency, based on which adaptive façade variants are assessed.

'The added value of coupling geometric design parameters directly to simulation software is (…) an important function that can help with the design' (Taveres-Cachat et al. 2021) of adaptive façades. The LiDICS method addresses this statement, as it encompasses not only model formation but also model coupling. The Functional Mock-up Interface (FMI) standard is employed as the exchange format. The primary goal of the FMI standard is to 'support the exchange of simulation models between suppliers and OEMs' (Blochwitz et al. 2011) for collaborative design and manufacturing while protecting intellectual property. The FMI standard offers advantages over Building Controls Virtual Test Bed (Wetter 2011) in that it 'provides a more streamlined

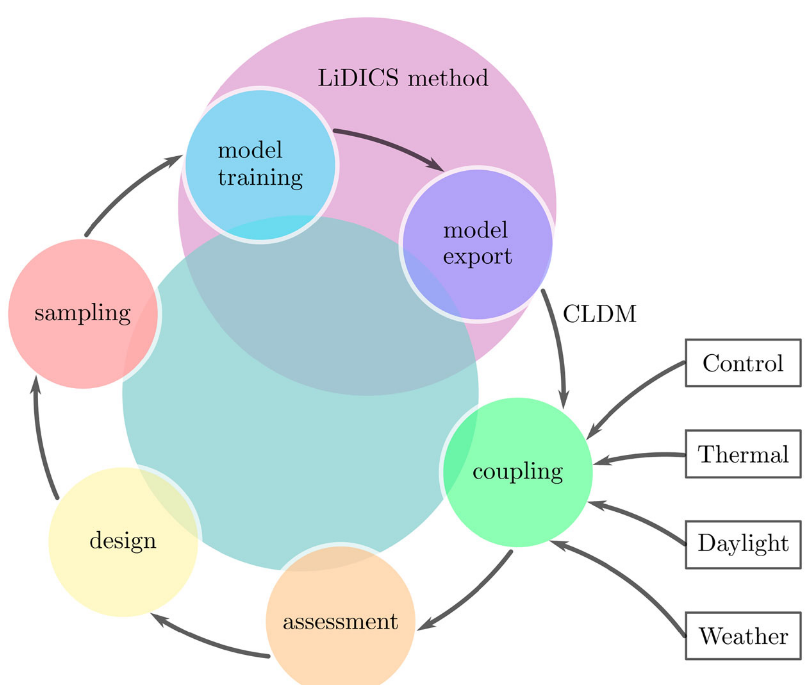

Figure 3. Flow diagram depicting the integration of the LiDICS method to the adaptive façade assessment workflow.

method for co-simulation' (Taveres-Cachat et al. 2021). The export of LiDICS based models into modular Functional Mock-up Units (FMU) facilitates a clear delineation of tasks and the exchange of models between architects, building physicists and control engineers. This means that LiDICS based façade models can be clearly compared, validated and delivered with the construction element as a digital twin. As an FMU model, it can be exchanged executably and accessed via a wide range of APIs, such as pyFMI. This step from an almost exclusively one-to-one to a standard interface coupling technique is one key feature that comes with the LiDICS methodology.

Key contributions

This work introduces the novel LiDICS methodical and model based interface that transforms ray tracing results into a FMU model. Its key features are:

- Realisation of continuous adjustable material and geometric properties. There is no need to restart the simulation or exchange the transmission matrix as required by the matrix based methods.
- The model is presented as a twice continuously differentiable function, thus it can be operated using existing optimal control concepts.
- Ease of model transferability as an executable FMU file into other multi domain simulation tools. Subsequent domain knowledge is not required.
- Ease of adaptation to different weather data and locations.
- Ease of building orientation modification for parameter variation.

Section 2 elucidates the adaptive façade assessment workflow and the fundamental mathematical principles of the LiDICS method. It also presents the model training and export process, along with a general validation.

Subsequently, Section 3 exemplifies the application of the method to switchable membrane cushion constructions. Herein, the initial four steps of the assessment workflow are demonstrated, encompassing the design, sampling, as well as model training and export. The following subsection explores the extent to which the outcomes derived from model training can be extrapolated to real-world weather data and locations. It represents an inter-model comparison with the RADIANCE 3-phase method. Finally, a potential analysis is conducted.

Chapter 4 concludes this work by presenting a summary of findings.

2. Methods

The LiDICS methodology is considered as one component within the comprehensive assessment workflow for adaptive façades. The initial subsection outlines the entire workflow, wherein the LiDICS methodology comprises two steps: model training and model export. Subsequent to the presentation of the general fundamentals in the second subsection, these workflow steps are elaborated in dedicated subsections. Finally, preliminary general validation procedures are undertaken.

2.1. Integration into the assessment workflow of adaptive façade variants

The comprehensive workflow is illustrated in Figure 3. The initial step involves defining the design of the construction variant. This entails mapping material properties to the geometrical surfaces. Along establishing the light quantities to be controlled, the façade inputs are defined. In the second step, the quantities are sampled for discrete sky conditions and façade inputs.

In the third step, the model is trained, resulting in the core matrices $\mathcal{P}$. This has been implemented in Python. Subsequently, the CLDM model is generated in Modelica using those core matrices and exported as an FMU file. These two steps will be described in greater detail below.

In the fifth step, the exported CLDM model is coupled with the model *Control* as well as the domain-specific models *Thermal* and *Daylight*, as illustrated in Figure 1. Furthermore, site-specific information, e.g. weather data, are incorporated for the first time. Finally, the construction variant is examined within annual simulations, from which key metrics for comfort, in multiple domains, and energy efficiency can be derived.

2.2. General fundamentals

$$q = \int_{\phi_w=0}^{2\pi} \int_{\theta_w=0}^{\pi/2} L(\theta_w, \phi_w) \mathrm{SIOP}\,(\theta_w, \phi_w, \vec{u}_{fac})\, \mathrm{d}\Omega_w \tag{1}$$

$$\mathrm{SIOP}\,(\theta_w, \phi_w, \vec{u}_{fac}) = \vec{Y}^T(\theta_w, \phi_w)\vec{s}(\vec{u}_{fac}) \quad \vec{s}, \vec{Y} \in \Re^{p_1} \tag{2}$$

$$Y_{l^2+l+m+1} = \tilde{Y}_l^m \quad \forall\, l \in [0, l_{\max}] \wedge m \in [-l, l] \tag{3}$$

$$q = \int_{\phi_w=0}^{2\pi} \int_{\theta_w=0}^{\pi/2} L(\theta_w, \phi_w)\vec{Y}^T(\theta_w, \phi_w)\, \mathrm{d}\Omega_w\, \vec{s}(\vec{u}_{fac}) \tag{4}$$

$$= \vec{e}^T\vec{s} \tag{5}$$

Within this section, the derivation of the mathematical foundations of the LiDICS model interface is presented. For this purpose, the relationship for the solar incidence operator (SIOP), Equation (2), is substituted into the hemispherical integral Equation (1). The double integral is written within the window coordinate system. Initially, the solar angles θ_a, ϕ_a are transformed from world into the window coordinate system θ_w, ϕ_w utilizing the slope β and azimuth angle γ of the reference surface. The convention of the coordinate systems and the coordinate conversion is carried out according to the studies (Rüdisser 2023; Schöttl 2013). The SIOP is the central variable representing the dependence of a quantity on the incidence angles and façade inputs. This formulation introduces a separation approach between the influences of the façade inputs $\vec{u}_{fac}$ within the expansion coefficient $\vec{s}$ and the influences of the zenith and azimuth angles within the spherical harmonics basis $\vec{Y}$. This separation approach was initially introduced in the foundational thesis (Rüdisser 2023) and further developed in this work to clarify the impact of multi-dimensional façade input $\vec{u}_{fac}$. The vector of spherical harmonic bases $\vec{Y}$ is determined using scaled cartesian harmonics $\tilde{Y}_l^m$ from the work (Bigi et al. 2023), with the prefactor F_l^m calculated iteratively. Since this has not yet been implemented in Modelica, validation is carried out in Subsection 2.5. The maximum dimension l_{max} is set to 12 in this work, leading to a feature dimension $p_1 = 169$.

This allows the general Equation (1) to be separated in two parts, cf. Equation (5), the problem specific expansion vector $\vec{s}$ and the vector of sky condition features $\vec{e}$ that is only dependent on the solar disturbance $\vec{d}_{sol}$.

Hemispherical integration

In this subsection, the determination of the vector $\vec{e}$ is presented for the first time. The assumption of a sky model is a prerequisite for its continuous representation. In this work, the Perez sky model from thesis (Rüdisser 2023, Section 6.2.3.2.) is applied. The solution of Equation (6) to (7) is carried out under the assumption of constant radiance regions L. For simplicity, $d\Omega_w$ is not expressed as $d\Omega_w = \sin(\theta_w)\,\mathrm{d}\theta_w\,\mathrm{d}\phi_w$. Terms (8) to (11) are taken from the work (Rüdisser 2023). Equation (12) describes the integral vectors $\vec{f}_i$. They are determined using the scipy routine *integrate.dblquad* and supplied in the supplemental material. The applied integration limits are dependent on the tilt angle of the reference surface β and can be found in Appendix 2. The index *i* represents the region of either sky (sky), ground (gnd) or horizon band (hor).

$$\vec{e} = \int_{\phi_w=0}^{2\pi} \int_{\theta_w=0}^{\pi/2} L(\theta_w, \phi_w)\vec{Y}(\theta_w, \phi_w)\,\mathrm{d}\Omega_w \tag{6}$$

$$= I_{dir}\vec{Y} + I_{cir}\vec{Y} + L_{sky}\vec{f}_{sky} + L_{hor}\vec{f}_{hor} + L_{gnd}\vec{f}_{gnd} \tag{7}$$

$$I_{cir} = I_{dif}F_1 \frac{1}{\max(\cos(85^\circ), \cos(\theta_a))} \tag{8}$$

$$L_{sky} = I_{dif}(1 - F_1)\frac{1}{\pi} \tag{9}$$

$$L_{hor} = I_{dif}F_2 4.426 \tag{10}$$

$$L_{gnd} = I_{glo}\alpha\frac{1}{\pi} \tag{11}$$

$$\vec{f}_i = \int_{\phi_w=0}^{2\pi} \int_{\theta_w=\theta_{i,lb}}^{\theta_{i,ub}} \vec{Y}(\theta_w, \phi_w)\,\mathrm{d}\Omega_w \tag{12}$$

2.3. Model training

The model training method proposed in this work is called incidence operator regularization (IOR). It is carried out after the sampling step. That involves the domain specific pre-simulation of all quantities for defined n_1 sky conditions, meaning discrete solar disturbances $\vec{d}_{sol}$, and n_2 discrete façade input points. When conducting the pre-simulation methods, such as 3-phase method, care should be taken to sample direct sky conditions and evenly distributed incidence angles. Then, this information is available in the measurement matrix $\mathcal{Q}$ for each quantity.

In the first step, the regression problem (13) with n_2 targets is solved. The matrix $\mathcal{E}$ is derived by evaluating Equation (7) for all n_1 samples. Each sample is associated with the solar disturbance $\vec{d}_{sol}$ that consists of the incidence angles θ_a, ϕ_a, the irradiance components $I_{dir}, I_{dif}, I_{glo}$, and the Perez parameters F_1, F_2. The albedo is always kept constant at $\alpha = 0.2$.

The result matrix $\mathcal{S}$ is then used for the second regression problem (14) with p_1 targets. The matrix $\mathcal{M}$ is generated by evaluating the basis function vector $\vec{\mu}$ for each of the n_2 discrete façade input points. In this work, due to the one-dimensional façade input u_{fac}, the basis function vector $\vec{\mu}$ is calculated using a one-dimensional Taylor expansion of degree $p_2 = 5$.

After solving the second regression problem, Equation (5) can be finalized to (16). The only output provided to the model export is the matrix $\mathcal{P}$ for each quantity.

$$\mathcal{Q} = \mathcal{E}\mathcal{S} \quad \mathcal{Q} \in \Re^{n_1 \times n_2}, \quad \mathcal{E} \in \Re^{n_1 \times p_1}, \ \mathcal{S} \in \Re^{p_1 \times n_2} \tag{13}$$

$$\mathcal{S}^T = \mathcal{M}\mathcal{P}^T \quad \mathcal{M} \in \Re^{n_2 \times p_2}, \ \mathcal{P} \in \Re^{p_1 \times p_2} \tag{14}$$

$$\vec{s} = \mathcal{P}\vec{\mu} \quad \vec{\mu} \in \Re^{p_2} \tag{15}$$

$$q = \vec{e}^T \mathcal{P}\vec{\mu} \tag{16}$$

To prevent overfitting during the first regression step, regularization methods are applied. The general formulation is designed for efficient and highly parallelized routines. Unlike the specific L0 regularization methodology used in the base study (Rüdisser 2023), this work employs the sklearn routine *linear_model.MultiTaskLassoCV* with a fold number of 5. This method efficiently solves the multi-target problem within a few seconds while simultaneously reducing the number of non zero entries.

For the second regression step, the sklearn routine *linear_model.LinearRegression* is used. Overfitting is not expected here, as the number of polynomial features $p_2 = 5$ does not exceed the number of samples $n_2 = 5$ in this work.

2.4. Model export

Figure 4 illustrates the CLDM Modelica model. The feature vectors $\vec{e}$ and $\vec{\mu}$ are generated according to the previous chapters. Then, these vectors are multiplied with the core matrix $\mathcal{P}$ for each quantity using Equation (17). The FMU model is generated by exporting the Modelica model.

$$q_i = \vec{e}^T \mathcal{P}_i \vec{\mu} \quad \forall\, i \in [1, o] \tag{17}$$

2.5. General validations

This subsection is intended to ensure that the FMU model delivers valid results regardless of the subsequent problem. The validation is divided into three steps.

The pivotal function of the Modelica component is the modelling of spherical harmonics in the vector $\vec{Y}$. This is the first validation step. This intricate function has not been previously implemented in Modelica. In this study, three formulations are integrated and juxtaposed with the results obtained from the Python implementation of scaled cartesian harmonics (Bigi et al. 2023, Equation 5ff). All formulations represent real-valued spherical harmonics. The first formulation adheres to the classical formulation (Bigi et al. 2023, Equation 2ff) in spherical coordinates. Similarly, the second formulation also follows spherical coordinates but computes the prefactor F_l^m using the iterative equation (Bigi et al. 2023, Equation C1). The third formulation employs scaled cartesian harmonics (Bigi et al. 2023, Equation 5ff) in cartesian coordinates, with the prefactor F_l^m determined iteratively as well. For validation purposes, all basis functions up to the index $l_{\max} = 12$, meaning $p_1 = 169$ features, are examined for a spiral trajectory of the spherical coordinates encompassing a total of 20,000 points. Figure 5 illustrates the mean absolute percentage error for all three formulations across the different features j. To calculate it, all values equal to zero are removed.

In the first formulation, depicted in Figure 5(a), no iteration equation is employed for the prefactor F_l^m. At higher indices j, the error increases sharply. This is attributed to the factorial increase surpassing the numerical storage capacity in Modelica. Conversely, the second formulation exhibits good agreement. In contrast, the third formulation shows an exact match or no absolute percentage deviation up to the range of 1e−18. Consequently, the third formulation is selected for subsequent use.

The second validation step is made to the generation of vector $\vec{e}$. In order to ensure the same solar disturbance $\vec{d}_{sol}$ for the Python and Modelica routines, their annual values have been generated with the widely adopted Modelica Buildings library (Wetter et al. 2014) for the location of the D1244 adaptive high-rise location and exported to Python.

Figure 6 depicts the mean absolute percentage error of the Python to FMU evaluation of $\vec{e}$ for different surface inclinations. There are errors between Python and FMU evaluation, but they are very low and could potentially be due to numerical precision.

As a third general validation step, the output of the total CLDM model is validated. The comparison is made against the global irradiance on tilted surface calculated using the Modelica Buildings library. To set up the CLDM, the solution matrix $\mathcal{P}$ was set to an array of zeroes except of the third entry of the first column. This value was set to the inverse of the third spherical harmonics prefactor $F_1^0 = \sqrt{\frac{3}{4\pi}}$. This represents a pure cosine behaviour according to the Lambertian absorption. To calculate

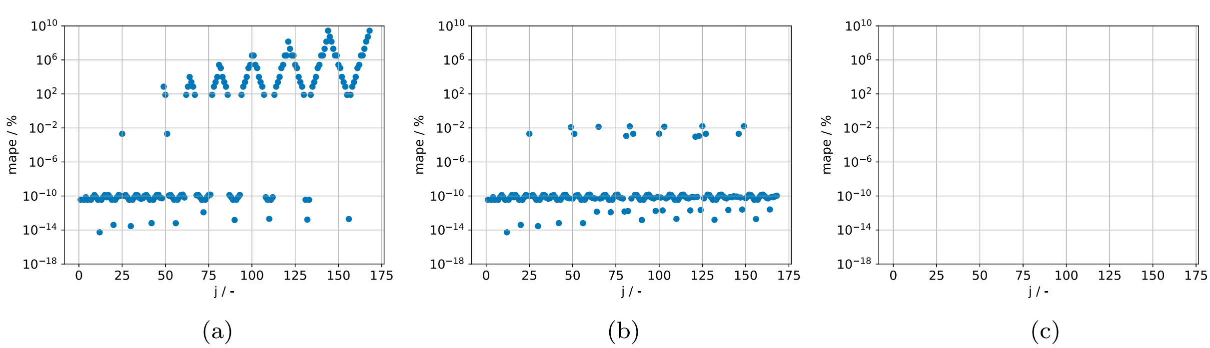

Figure 5. Mean absolute percentage error between Python and FMU evaluation of spherical harmonics for different bases and three formulations. (a) Spherical formulation. (b) Spherical formulation plus iterative prefactor F_m^l. (c) Cartesian formulation plus iterative prefactor F_m^l.

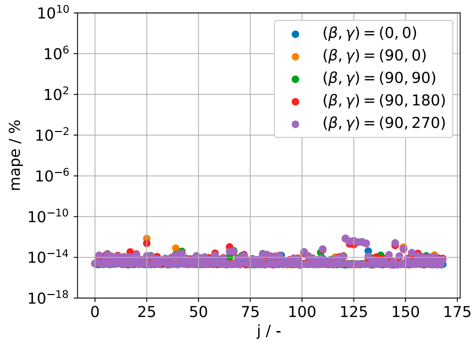

Figure 6. Mean absolute percentage error between Python and FMU evaluation of $\vec{e}$ for different bases and surface inclinations.

Table 1. Validating Modelica CLDM model with Modelica Buildings library by annual irradiance on inclined planes applying metrics maximum error (me), mean absolute error (mae) und mean absolute percentage error (mape).

β / °	γ / °	me / $\frac{W}{m^2}$	mae / $\frac{W}{m^2}$	mape / %
0	0	6.7	1.8	1.0
90	0	0.1	0.0	0.0
90	90	0.2	0.0	0.0
90	180	0.1	0.0	0.0
90	−90	0.2	0.0	0.0

the mean absolute percentage error, all zero values are removed.

Table 1 shows the results for different inclinations. Negligibly small deviations ($mape = 1\%$) occur only for an inclination angle of $\beta = 0°$. This deviation is due to the difference in the mapping of the horizon band. The Perez model assumes an infinitesimal horizon line, which is scaled here to zero with $\sin(\beta)$. The LiDICS model, on the other hand, uses the actual integral value here. For the other inclinations, there are no deviations.

Table 2. Spectral data of the transparent and printed regions of the stripe pattern.

in %	τ_v	$\rho_{f,v}$	$\rho_{b,v}$	τ_s	$\rho_{f,s}$	$\rho_{b,s}$	τ_{ir}	$\varepsilon_{f,ir}$	$\varepsilon_{b,ir}$
transparent	89	9	9	90	8	9	7	89	88
printed	5	56	59	5	56	59	1	91	44

3. Application to switchable membrane cushion constructions

In this section, the first five steps of the proposed workflow, cf. Figure 3 are applied to a switchable membrane cushion, as depicted in Figure 7. Following the assumptions made in ISO 52022-3 and the Klems matrix layer method, a plane-parallel layer structure is assumed. The membrane construction comprises three layers, with only the first two membrane layers printed with a horizontal and complementary stripe pattern. The integral shortwave spectral properties of the printed and transparent regions are determined experimentally and are provided in Table 2. Infrared data was interpolated using the measurement data from the study (Haase et al. 2019, Table 9).

Due to its three layer construction, the structure has two air chambers and consequently two independent façade inputs, cf. Figure 7(c). Additionally, it is assumed that the distance l_{23} has no influence on the light dynamics, as it only involves moving a highly transparent layer. Nevertheless, this distance is considered in the thermal modelling. Consequently, the light dynamics exhibit one-dimensional dependency. The façade input $u_{fac} = \frac{l_{12}}{l_{13}}$ is the percentage layer distance l_{12} in relation to a maximum distance of $l_{13} = 50\,\text{cm}$.

The room exhibits a typical shoebox geometry with dimensions of 3.6 m × 2.8 m × 8.2 m (WxHxD), as outlined in the study (Reinhart, Jakubiec, and Ibarra 2013). Weather data for the D1244 adaptive high-rise location

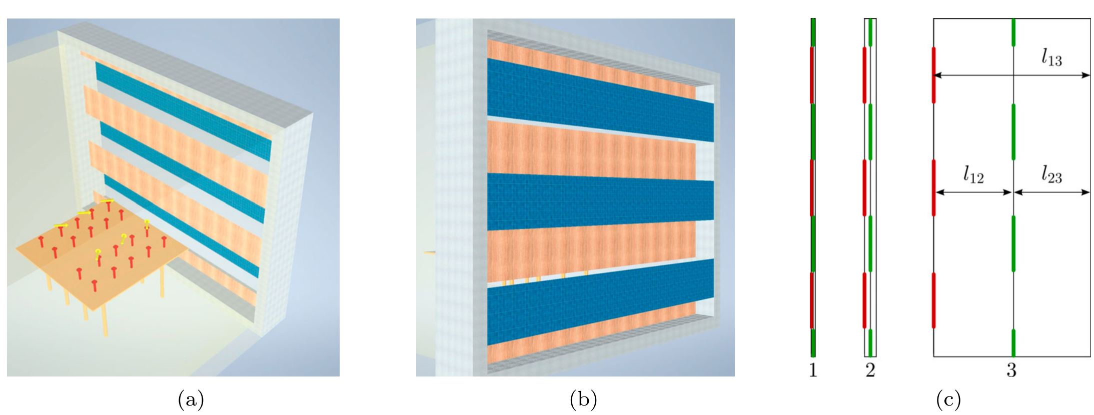

Figure 7. Design of the switchable three layer membrane cushion construction with stripe pattern. The pattern regions are colored orange and blue for better visibility. Transparent regions are kept invisible. The switching mechanism is shown for the three thermally relevant states (1: conductive, 2: insulating, 3: insulating with transmission). (a) Indoor view (b) Ambient view (c) Switching mechanism.

(48.749°N, 9.112°E) is sourced from the Meteonorm software.

3.1. Design & sampling

The assessment workflow starts with the design and material mapping. After that a total of four solar and 26 visual quantities are identified. The solar quantities encompass the absorptions of the three layers and the transmission. The visual quantities represent the illuminance on the 26 sensors illustrated in Figure 7(a). The positions of these sensors are provided in the supplementary material. In step two the façade input is divided into five ($n_2 = 5$) discrete points $u_{fac,d} = \{0, 25, 50, 75, 100\}\%$ from totally closed to totally open.

Angle-dependent solar quantities are generated with the LBNL method. First, the BSDF of each membrane layer is generated using RADIANCE for the solar spectrum range. The angle-dependent quantities are subsequently determined using the Klems matrix layer method in WINDOW. Consequently, only $n_1 = 145$ angle pairs are employed for the incidence operator regularization. The data are supplied in the window coordinate system. The window is later assumed to be inclined by a slope $\beta = 90°$ in the system simulation. Therefore, the matrix $\mathcal{E}$ must be generated using the same slope, a direct normal irradiance $I_{dir} = 1\frac{W}{m^2}$ and without any diffuse and global horizontal $I_{dif} = I_{glo} = 0$ irradiance.

Angle-dependent illuminance values are generated applying the RADIANCE 3-phase method for $n_1 = 1000$ randomly distributed solar incidence angle pairs over the hemisphere. The daylight simulations are carried out without diffuse horizontal irradiance but a direct normal irradiance of $I_{dir} = 1000\frac{W}{m^2}$, a global horizontal irradiance of $I_{glo} = \cos(\theta_a)I_{dir}$ and standard albedo of $\alpha = 0.2$. As the simulations are carried out in the world system the coordinate transformation must be applied.

In general, all matrices $\mathcal{E}$ for all quantities must be generated with the same inclination of the reference surface. In this work, an inclination angle of $\beta = 90°$ is used for the incidence operator regularization. The SIOPs are defined exclusively in the window coordinate system and vary depending on the previously set inclination angle of the reference surface. These investigations suggest that an inclination of 0° is more suitable for visualizing shading situations in building ensembles, while an inclination of 90° is more suitable for component analysis.

3.2. Model training & export

According to step three of the proposed workflow, the two stage incidence operator regularization is conducted. Within the first stage, see Equation (13), the matrix $\mathcal{S}$ is determined for all quantities. The model quality is assessed using Equation (18).

$$y_{true} = \mathcal{Q} \quad y_{pred} = \mathcal{E}\mathcal{S} \tag{18}$$

The first regularization stage for all 30 quantities requires a computation time of 56 seconds. A median coefficient of determination of $r^2 = 99.4\%$ was achieved for the training data. There is one outlier for the quantity transmission (T), as shown in Figure 8.

This reveals that the achieved accuracy is not related to the number of non zero elements, which corresponds to the complexity of the angular dependence. The visual quantities (E1–E26) require many coefficients and achieve high accuracy. The quantities A1 and A2 exhibit predominantly Lambertian absorption behaviour and require only few coefficients for high accuracy. This indicates that the solver can effectively regularize both simple and complex angular dependencies. However, the quantity T cannot be well regularized. This could be due to several factors. Firstly, there is a relatively small number of samples ($n_1 = 145$) in combination with a higher angular dependence. Secondly, the data for T contain errors that could be related to the execution of the LBNL method.

A more detailed analysis of the outlier is shown in Figure 9. This figure illustrates the solar incidence operator for the quantity transmission (T) with a fully open façade ($u_{fac} = 100\%$) and compares Lasso and Ridge regularization results. While the latter does achieve an improvement in accuracy from $r^2 = 83\%$ to $r^2 = 98\%$, it comes at the cost of overfitting the data, leading to angular dependencies that are not physically plausible. Given that the printing pattern is symmetrically arranged, the incidence operators should exhibit symmetry. In contrast, Lasso regularization results in a more physically consistent behaviour. This type of visualization could also be used in the future to validate the fundamental generation methods of the quantities.

$$y_{true} = \mathcal{S}^T \quad y_{pred} = \mathcal{M}\mathcal{P}^T \tag{19}$$

The second regularization stage, see Equation (14), represents the interpolation between the discrete façade inputs. The model quality is assessed using Equation (19). In this context, Figure 8(c) shows the model quality of the second regression for all quantities. It consistently achieves 100% accuracy, indicating that no errors arise from the interpolation between the discrete façade inputs.

For the fourth workflow step, the model export, the FMU model was created using the procedure presented in Subsection 2.4.

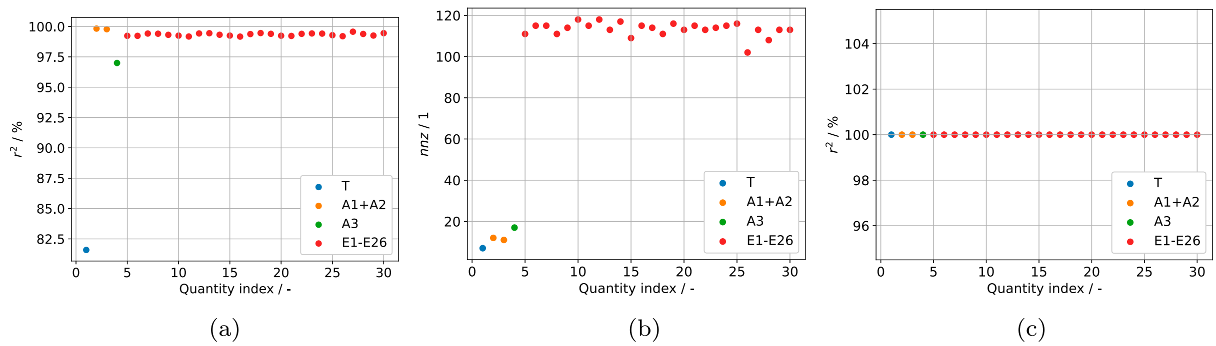

Figure 8. Model training results for all quantities. (a) r^2 of regularization step 1 (b) Number of non zero rows of $\mathcal{S}$, $\mathcal{P}$ (c) r^2 of regularization step 2

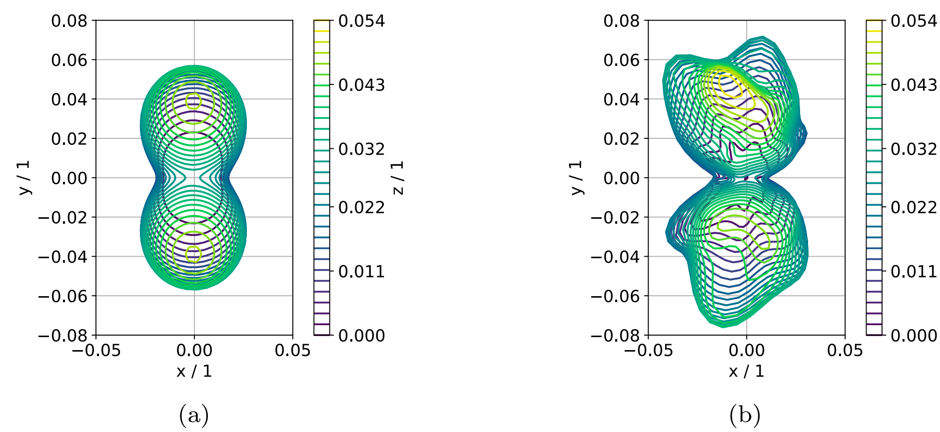

Figure 9. Comparing two regularization methods for quantity solar transmission (T) and façade input ($u_{fac} = 100\%$). (a) Lasso regularization, $r^2 = 83\%$ (b) Ridge regularization, $r^2 = 98\%$.

3.3. Application specific validation

In this section, it is tested whether the model derived from the previous subsection can be transferred to real-world weather data and locations. This inter-model comparison is carried out with the RADIANCE 3-phase method in hourly resolution ($n_1 = 8760$) and each discrete façade input ($n_2 = 5$) at the location of the D1244 high-rise building with its azimuth orientation ($\gamma = -20^\circ$). From these simulations, the matrix $\mathcal{Q}'$ is obtained. It is important that the matrix $\mathcal{E}'$ is created with the inclination angle $\beta = 90^\circ$ and the azimuth angle $\gamma = -20^\circ$. The comparison is conducted only for the visual quantities. The metrics are determined using Equation (20). To ensure the determination of the mean absolute percentage error, only brightness values greater zero lux are used.

$$y_{true} = \mathcal{Q}' \quad y_{pred} = \mathcal{E}'\mathcal{P}\mathcal{M}^T \tag{20}$$

Figure 10 allows for two comparisons: one between the LiDICS model and the RADIANCE 3-phase method, and the other between the implementation of Equation (17) in Python and in the FMU model.

The comparison between the Python and FMU evaluation reveals that the Python evaluation consistently demonstrates higher accuracy. Across all quantities, the coefficient of determination is superior, the mean absolute error is lower, and consequently, the mean absolute percentage error is lower. Compared to the results from the previous general validation, cf. Subsection 2.5, the addition of the problem-specific matrices $\mathcal{P}$ has increased the differences between the Python and FMU evaluation. The reason for this remains unclear. Perhaps small numerical differences within the matrix $\mathcal{P}$ have a strong effect.

Turning to the comparison between the Python evaluation and the RADIANCE 3-phase method, we observe a median coefficient of determination of 98.5%, a mean absolute error of 32 lux and a mean absolute percentage error of 11.6% on all quantities. This consistently indicates a high degree of accuracy in the LiDICS model. Therefore, the hypothesis holds that the matrix $\mathcal{P}$, trained using the results from the sampling step, can be transferred to real-world weather data and locations.

Additionally, Figure 11 provides a visual assessment of the deviation between the LiDICS model and the 3-phase method. It compares a 10-day segment of illuminance from workplace sensor 1 for a fully open façade ($u_{fac} =$

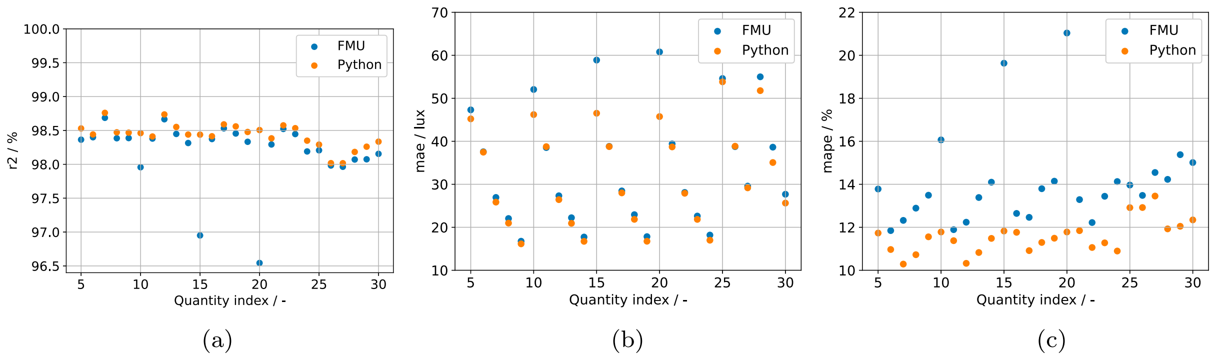

Figure 10. Comparison of annual illuminance between 3-phase-method and LiDICS depicted for FMU and Python evaluation of Equation (17). (a) Coefficient of determination (b) Mean absolute error (c) Mean absolute percentage error.

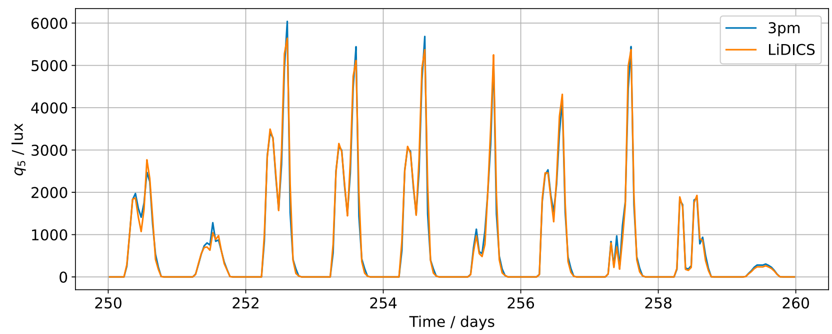

Figure 11. Exemplary 10 days trajectory of 3-phase method and LiDICS for workplace sensor 1 with fully opened façade ($u_{fac} = 100\%$) on hourly resolution.

100%). This comparison further supports the high accuracy of the LiDICS methodology. Possible discrepancies might arise from differences in the interpolation between the solar angles within the two methods. Beyond the excellent agreement and the associated transferability, the LiDICS method offers two other significant advantages. Firstly, adjusting the façade azimuth does not require the creation of a new sky matrix, allowing for the consideration of all window orientations. Secondly, the lighting behaviour can be continuously adjusted with the façade input, eliminating the need to interrupt the simulation and reinitialise with another transmission matrix, as required by the 3-phase method. This will be demonstrated in the following chapter.

3.4. Potential analysis

Finally, the potential of the LiDICS model interface for coupled optical and thermal simulation is briefly demonstrated. The meteorological data and the azimuth orientation of the room have been configured as described in the preceding chapters. The overall model is structured as illustrated in Figure 1 and established in Modelica.

In the thermal model, solar heat flows are directed into the thermal resistance network of the façade, as

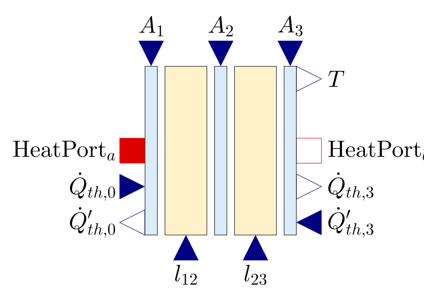

Figure 12. Thermal façade model of the switchable membrane cushion.

depicted in Figure 12. The equations from ISO 52022-3 have been adapted such that the heat flows from short wave absorption and transmission are not determined internally through iterative calculation but are externally added to the network. Furthermore, the thermal gap resistances are modelled time-variant. A thickness of 250 μm and a thermal conductivity of $\lambda = 0.24 \frac{W}{mK}$ are assumed for each membrane layer. A constant room temperature of 25°C has been set.

Within the daylight model, the mean workplace illuminance is determined from all sensors located at the two workstations. The simplified daylight glare probability is calculated from the maximum of all six sensors at eye level.

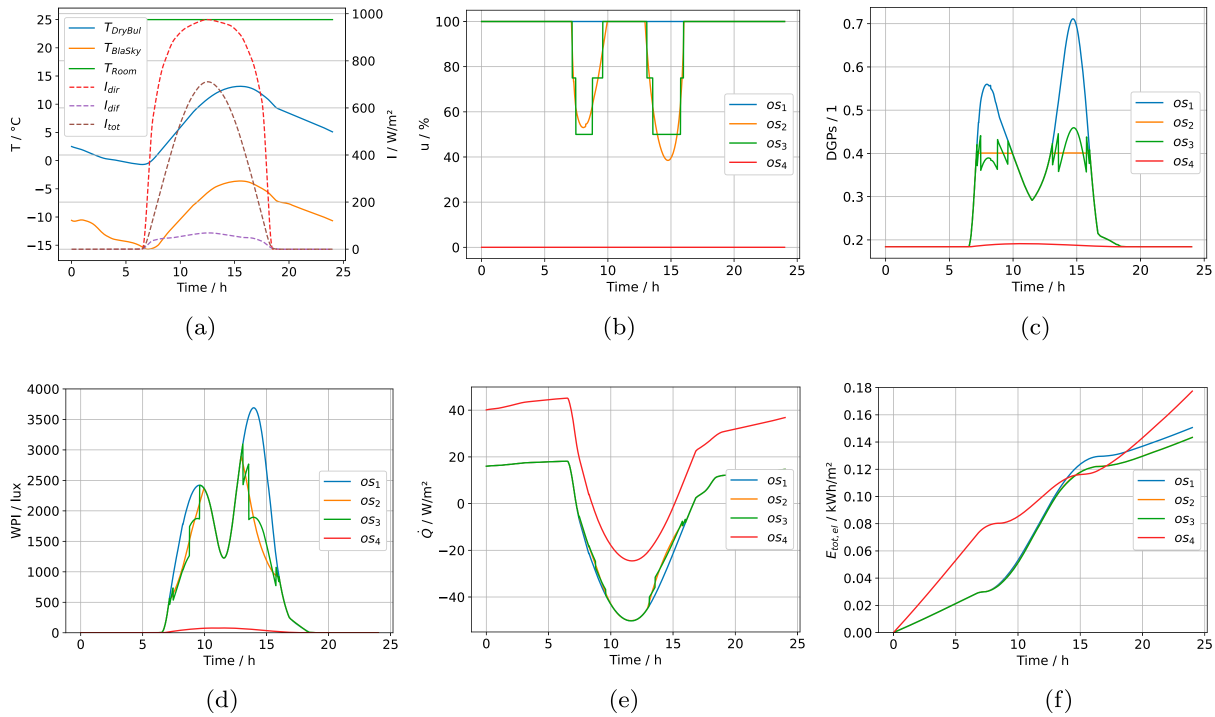

Figure 13. Time series of weather data and system variables for four different operation strategies *os*. (a) weather data (b) façade input (c) simple daylight glare probability (d) workplace illuminance (e) thermal power (f) electrical energy consumption.

Figure 13 depicts the time series of weather data for a selected spring day with intense direct solar irradiance and various system variables for four different operational strategies. All strategies set both layer distances equal to $l_{12} = l_{23} = u_{fac} l_{13}$. The strategy os_1 maintains the façade input constantly open at $u_{fac} = 100\%$. The strategy os_4 maintains the façade opening constantly closed at $u_{fac} = 0\%$. The strategy os_2 controls the façade opening using a proportional controller, ensuring that the glare potential does not exceed a perceptible and mainly not disturbing value $DGPs = 0.4$ according to DIN EN 14501. The operational strategy os_3 illustrates the control between discrete façade openings by mapping the trajectory of operational strategy os_2 to the five discrete façade inputs. The electrical energy consumption was calculated with a coefficient of performance $cop = 4$ and an energy efficiency ratio $eer = 3$.

Figure 13(c) illustrates the simplified glare potential. Operational strategy os_2 successfully limits the glare potential to the comfortable value, compared to other strategies. The selection of discrete façade states in os_3 results in a discontinuous trajectory of the system variables. Consequently, the comfort limit can only be guaranteed by setting an even smaller façade opening, which in turn would affect other system variables. This clearly demonstrates the implementation and advantage of a continuous adjustable geometric property with the LiDICS model.

The analysis of the thermal performance of the electrical energy consumption highlights the potential of the switchable membrane cushion construction. As with strategy os_4, when all air is removed from the construction, a high U-value of the construction occurs. This leads to reduced cooling energy consumption on cold spring days with high solar heat gains, as cooling can be achieved through the façade. However, this also reduces light transmission. The application of optimal control concepts could advantageously exploit the potential of standard insulation at night and high conductivity during the day, at least on a temporary or occupancy based level.

Overall, this brief example demonstrates that the application of the LiDICS method allows for a coupled analysis of the effects of continuous façade actuation on the thermal and daylight domains from control development perspective.

4. Conclusion

This work addresses the challenges of performance assessment for adaptive façades. This includes the representation of adjustable material and geometric properties within a building performance simulation.

To this end, the novel LiDICS methodical and model based interface is introduced. The necessary assessment workflow for adaptive façades, as well as the mathematical foundations of the model, are derived in the methodology section. The LiDICS method is positioned as an interface within the presented adaptive façade assessment workflow, situated between ray tracing based sampling and subsequent multi-domain coupling. It comprises two principal steps; model training and export. The model training transforms sampling outcomes into an algebraic model using the novel two-stage incidence operator regularization. Then, the model is exported as a Functional Mock-up Unit.

This approach enables, firstly, the continuous adaptation of material and geometric properties, and secondly, the integration of complex light dynamics into a variety of building performance simulation tools with a standard coupling interface. Consequently, the presented approach offers a solution to a central challenge in the performance assessment of adaptive façades.

In the second part of this thesis, the LiDICS method was applied to a three layered switchable membrane cushion construction featuring a complementary printing pattern. When closed, the construction forms a continuously reflective surface; otherwise, light can enter at an angle. As only layers 1 and 2 are printed, it is assumed that only the distance between layer 1 and layer 2 influences the light dynamics. This distance represents the adjustable geometric property or façade input and was discretized into five points. The solar quantities represent the layer absorptions and the transmission. They were determined using the LBNL method for 145 discrete sky positions and five discrete façade input points. The visual quantities represent 26 illuminance sensors within the room. These were determined using the 3-phase method for 1000 discrete sky positions and five discrete façade input points.

The model training requires negligible computational time, less than one minute, and achieves high accuracy ($r^2 = 99.4\%$). The newly developed feature basis $\vec{e}$ is therefore suitable for representing highly angle-dependent light dynamics.

Subsequently, an inter-model validation step was conducted. The model generated using the LiDICS method was compared with annual simulations using the 3-phase method. The validation step also achieves high accuracy with a median coefficient of determination of 98.4% and a mean absolute deviation of 31 lux across all visual quantities.

Finally, the potential of the adjustable geometric properties of the resulting model was investigated. To this end, it was coupled with a thermal and a daylight model. A simple proportional controller was designed to maintain glare below a perceptible and mainly not disturbing value. In comparison to a discrete selection of façade entry points, adherence to the comfort limit can be guaranteed. This highlights that material and geometric properties are adjustable with the LiDICS method.

4.1. Future work

Future studies could utilize this model to develop optimal control strategies for coupled optical and thermal problems.

After the first stage of the incidence operator regularization, the SIOP surface distorts towards the pre-simulated points. The points differ significantly in their geodesic distance on the SIOP surface. This results in these values being underrepresented in the regularization, even though they have a high SIOP value and substantial impact on the integral value. Future work could address this issue by determining the geodesic distance between all pre-simulated points on the SIOP surface and incorporating these into a regression scheme with iterative reweighting. Additionally, resampling of underrepresented regions could potentially be included.

The second regression stage is currently designed for one-dimensional façade inputs. Future work could incorporate the multivariate influence using appropriate feature bases. This could also be achieved through general machine learning concepts. In doing so, there should always be a focus on the twice continuous differentiability of the underlying models.

In this work, the first IOR stage was further carried out, as a model identification, with the matrices $\mathcal{Q}'$ and $\mathcal{E}'$ using the annual simulation of the 3-phase method. The identified SIOPs are compared with those of the model training for error analysis. This principle could be applied to measurement data of illuminance values in order to derive more detailed glare informations and perhaps be compared to results from a luminance camera. Additionally, solar quantities could be indirectly identified with this approach from transient thermal measurements.

Presently, there is a lack of an end-to-end workflow from parametric design to the LiDCS model export. Generating dynamic models of angle-dependent light dynamics within a parametric design tool would be a useful feature. Through its reliance on the Python language, the LiDICS method significantly advances this integration.

CRediT author statement

Simon O. Weber: Conceptualisation, Methodology, Software, Validation, Formal analysis, Investigation, Resources, Data curation, Writing – Original draft, Visualisation.
Yuan Fang: Investigation, Resources, Writing – Review & Editing.
Daniel Rüdisser: Conceptualisation, Methodology, Writing – Review & Editing.

Philip Leistner: Writing – Review & Editing, Supervision, Project administration, Funding acquisition.

Declaration of Competing Interest and AI assistance

The authors declare that they have no known competing financial interests or personal relationships that could have appeared to influence the work reported in this paper. During the preparation of this paper the authors used generative AI and AI-assisted technologies, but only for translation and linguistic comprehensibility.

Data availability statement

In the supplementary materials, the file *fVec.csv* contains the solutions of Equation (12) for all sky types, spherical harmonics bases, and two slope angles. In addition to the sensor positions (*SensorPositions.csv*), which are defined in the world coordinate system, the dataframes *dfRaw.csv* and *dfRaw_3pm.csv* are also included. The latter contains the input matrices ($\mathcal{Q}$, $\mathcal{E}$, $\mathcal{M}$) for model training and model validation using the 3-phase method. The results of the model training ($\mathcal{S}$, $\mathcal{P}$) are provided in the dataframe *dfRes.csv*.Additionally, interactive 3D plots of the SIOPs of all quantities for all façade input points are provided. The supplemental material is available at the data repository of the University of Stuttgart https://doi.org/10.18419/darus-4107.

Funding

This work was supported by the German Research Foundation (DFG, Deutsche Forschungsgemeinschaft, Project-ID 279064222), as a part of the collaborative research center CRC1244 (SFB1244) "Adaptive Skins and Structures for the Built Environment of Tomorrow" sub-project C05 "Building Physical Adaptive Façades".

Nomenclature

Variables

Symbol	Description	Unit
o	number of quantities	1
p_1	number of features / predictors for IOR step 1	1
p_2	number of features / predictors for IOR step 2	1
n_1	number of samples for IOR step 1	1
n_2	number of samples for IOR step 2	1
α	albedo	1
β, γ	window slope and azimuth angle	°
θ, ϕ	zenith and azimuth angle	°
q	quantity	lux or W/m^2
u_{fac}	façade input	
d_{sol}	solar disturbance	
SIOP	solar incidence operator	1
L	radiance	$W/m^2/sr$
I	irradiance	W/m^2
Ω	solid angle	sr
s	series coefficient of spherical harmonics expansion	1 or $\frac{lm}{W}$
$Y_j, \tilde{Y}_l^m$	spherical harmonics base function	1
e	total hemispherical integrand	W/m^2
f	hemispherical integrand of spherical harmonic base	sr
F_1, F_2	Perez sky parameter	1
$\mathcal{Q}, \mathcal{E}, \mathcal{S}$	matrices for IOR step 1	
$\mathcal{S}, \mathcal{P}, \mathcal{M}$	matrices for IOR step 2	
l	gap width distance	cm
j, l, m	indices to describe one spherical harmonic base	
τ, ρ, ε	transmission, reflection, emission coefficient	%
nnz	number of non zero entries	1
me	maximum error metric	W/m^2
mae	mean absolute error metric	lux or W/m^2
mape	mean absolute percentage error metric	%
r^2	coefficient of determination	%

Subscripts

Symbol	Description
a, w	world and window coordinate system
dir, dif, glo	direct normal, diffuse horizontal, global horizontal irradiance
circ, hor, sky, gnd	circumsolar, horizon, sky, ground
v, s, ir	visual, solar and infra-red wavelength spectrum
f, b	front, back
12, 23, 13	distance between the layers 1,2 and 3

References

Bigi, Filippo, Guillaume Fraux, Nicholas J. Browning, and Michele Ceriotti. 2023. "Fast Evaluation of Spherical Harmonics with Sphericart." *The Journal of Chemical Physics* 159 (6): 064802. https://doi.org/10.1063/5.0156307.

Blandini, Lucio, Walter Haase, Stefanie Weidner, Michael Böhm, Timon Burghardt, Daniel Roth, Oliver Sawodny, and Werner Sobek. 2022. "D1244: Design and Construction of the First Adaptive High-Rise Experimental Building." *Frontiers in Built Environment* 8:814911. https://doi.org/10.3389/fbuil.2022.814911.

Blochwitz, T., M. Otter, M. Arnold, C. Bausch, C. Clauss, H. Elmqvist, A. Junghanns, et al. 2011. "The Functional Mockup Interface for Tool independent Exchange of Simulation Models." In *Proceedings 8th Modelica Conference*. Dresden, Germany.

Borkowski, Esther, Dimitrios Rovas, and Rokia Raslan. 2021. "Adaptive Building Envelope Simulation in Current Design Practice: Findings from Interviews with Practitioners about Their Understanding of Methods, Tools and Workarounds and Implications for Future Tool Developments." *Intelligent Buildings International* 14 (2): 172–189. https://doi.org/10.1080/17508975.2021.1902257.

Bueno, Bruno, Jose M. Cejudo-Lopez, and Tilmann E. Kuhn. 2017. "A General Method to Evaluate the Thermal Impact of Complex Fenestration Systems in Building Zones." *Energy and Buildings* 155:43–53. https://doi.org/10.1016/j.enbuild.2017.08.055.

Bueno, Bruno, Jan Wienold, Angelina Katsifaraki, and Tilmann E. Kuhn. 2015. "Fener: A Radiance-Based Modelling Approach to Assess the Thermal and Daylighting Performance of Complex Fenestration Systems in Office Spaces." *Energy and Buildings* 94:10–20. https://doi.org/10.1016/j.enbuild.2015.02.038.

Carlucci, Francesco, Roel C. G. M. Loonen, Francesco Fiorito, and Jan L. M. Hensen. 2023. "A Novel Approach to

Account for Shape-Morphing and Kinetic Shading Systems in Building Energy Performance Simulations." *Journal of Building Performance Simulation* 16 (3): 346–365. https://doi.org/10.1080/19401493.2022.2142294.

Coffey, Brian, Andrew McNeil, Thierry Nouidui, and Eleanor S. Lee. 2022. "Automated Production of Optimization-Based Control Logics for Dynamic Facade Systems, with Experimental Application to Two-Zone External Venetian Blinds." Technical report, Lawrence Berkeley National Lab. (LBNL), Berkeley, CA (United States).

Crespi, Manuela, and Sandra Giulia Linnea Persiani. 2019. "Rethinking Adaptive Building Skins from a Life Cycle Assessment Perspective." *Journal of Facade Design and Engineering* 7 (2): 21–43.

Curcija, Charlie, Simon Vidanovic, Robert Hart, Jacob Jonsson, and Rebecca Powles. 2018. "WINDOW Technical Documentation." Technical report.

de Vries, Samuel B., Roel C. G. M. Loonen, and Jan L. M. Hensen. 2021. "Multi-State Vertical-Blinds Solar Shading – Performance Assessment and Recommended Development Directions." *Journal of Building Engineering* 40:102743. https://doi.org/10.1016/j.jobe.2021.102743.

Favoino, Fabio, Roel Loonen, Maxime Doya, Francesco Goia, Chiara Bedon, and Francesco Babich. 2018. *Building Performance Simulation and Characterisation of Adaptive Facades – Adaptive Facades Network*. TU Delft Open for the COST Action 1403 adaptive facade network.

Ganji Kheybari, Abolfazl, Tim Steiner, Steven Liu, and Sabine Hoffmann. 2021. "Controlling Switchable Electrochromic Glazing for Energy Savings, Visual Comfort and Thermal Comfort: A Model Predictive Control." *CivilEng* 2 (4): 1019–1051. https://doi.org/10.3390/civileng2040055.

Gehbauer, Christoph, David H. Blum, Taoning Wang, and Eleanor S. Lee. 2020. "An Assessment of the Load Modifying Potential of Model Predictive Controlled Dynamic Facades within the California Context." *Energy and Buildings* 210:109762. https://doi.org/10.1016/j.enbuild.2020.109762.

Gehbauer, Christoph, Eleanor S. Lee, and Taoning Wang. 2023. "An Evaluation of the Demand Response Potential of Integrated Dynamic Window and HVAC Systems." *Energy and Buildings* 298:113481. https://doi.org/10.1016/j.enbuild.2023.113481.

Haase, Walter, Clemens Freitag, Andreas Kaufmann, Herbert Sinnesbichler, Matthias Kersken, Almuth Schade, Florian Hess, and Angela Püls. 2019. *Bewertungsverfahren Leichtbau: Entwicklung eines vereinfachten Bewertungsverfahren zur Bestimmung der wärmetechnischen Eigenschaften (U-Wert, g-Wert) von Membranhüllen-Konstruktionen*, Forschungsinitiative Zukunft Bau. Stuttgart: Fraunhofer IRB Verlag.

Klems, Joseph. 1993. "A New Method for Predicting the Solar Heat Gain of Complex Fenestration Systems II. Detailed Description of the Matrix Layer Calculation." *ASHRAE Transactions* 100: 1.

Kuhn, Tilmann E., Sebastian Herkel, Francesco Frontini, Paul Strachan, and Georgios Kokogiannakis. 2011. "Solar Control: A General Method for Modelling of Solar Gains through Complex Facades in Building Simulation Programs." *Energy and Buildings* 43 (1): 19–27. https://doi.org/10.1016/j.enbuild.2010.07.015.

Loonen, Roel C. G. M., Fabio Favoino, Jan L. M. Hensen, and Mauro Overend. 2017. "Review of Current Status, Requirements and Opportunities for Building Performance Simulation of Adaptive Facades." *Journal of Building Performance Simulation* 10 (2): 205–223. https://doi.org/10.1080/19401493.2016.1152303.

Molina, Germán. 2014. "Integrated Thermal and Lighting Analysis of Spaces with Controled Complex Fenestration Systems and Artificial Lighting During the Design Stage." PhD diss., Pontificia Universidad Catolica de Chile (Chile).

Reinhart, Christoph F., J. Alstan Jakubiec, and Diego Ibarra. 2013. "Definition of A Reference Office for Standardized Evaluations of Dynamic Façade and Lighting Technologies." In *13th Conference of International Building Performance Simulation Association*. Chambéry, France.

Rüdisser, Daniel. 2023. "RadiCal – A Novel Method to Model Energy Flows Induced by Solar Radiation." PhD diss.

Schöttl, Peter. 2013. "Integration Komplexer Verglasungssysteme mit Bidirectional Scattering Distribution Functions in TRNSYS."

Shen, Linhai, and Yunsong Han. 2022. "Optimizing the Modular Adaptive Façade Control Strategy in Open Office Space Using Integer Programming and Surrogate Modelling." *Energy and Buildings*254:111546. https://doi.org/10.1016/j.enbuild.2021.111546.

Tabadkani, Amir, Astrid Roetzel, Hong Xian Li, and Aris Tsangrassoulis. 2022. "Simulation-Based Personalized Real-Time Control of Adaptive Facades in Shared Office Spaces." *Automation in Construction* 138:104246. https://doi.org/10.1016/j.autcon.2022.104246.

Taveres-Cachat, Ellika, Fabio Favoino, Roel Loonen, and Francesco Goia. 2021. "Ten Questions concerning Co-Simulation for Performance Prediction of Advanced Building Envelopes." *Building and Environment*191:107570. https://doi.org/10.1016/j.buildenv.2020.107570.

UNEP, U. N. 2021. "2021 Global Status Report for Buildings and Construction." Technical report.

Vera, Sergio, Waldo Bustamante, Germán Molina, and Daniel Uribe. 2016. "A Flexible and Time-Efficient Schedule-Based Communication Tool for Integrated Lighting and Thermal Simulations of Spaces with Controlled Artificial Lighting and Complex Fenestration Systems." *Journal of Building Performance Simulation* 9 (4): 382–396. https://doi.org/10.1080/19401493.2015.1062556.

Vlachokostas, Alex, and Nicholas Madamopoulos. 2017. "Daylight and Thermal Harvesting Performance Evaluation of a Liquid Filled Prismatic Façade Using the Radiance Five-Phase Method and EnergyPlus." *Building and Environment* 126 (12): 396–409. https://doi.org/10.1016/j.buildenv.2017.10.017.

Ward, Gregory J. 1994. "The RADIANCE Lighting Simulation and Rendering System." In *Proceedings of the 21st Annual Conference on Computer Graphics and Interactive Techniques, SIGGRAPH '94*. New York, NY: Association for Computing Machinery.

Weber, Simon O., Yuan Fang, Sumee Park, and Philip Leistner. 2023a. "Analysis and Control of Cross-Domain Effects of Inhomogeneous Pattern on Switchable Membrane Constructions (Accepted)." In *Bright Environments: Daylight in Sustainable Building Design Conference*. Zurich, Switzerland.

Weber, Simon O., Yuan Fang, Sumee Park, and Philip Leistner. 2023b. "Sequentially Coupling LBNL-Method and Modelica to Model and Operate Adaptive Facades with Inhomogeneous Printing Patterns." In *Journal of Physics: Conference Series*. Lausanne, Switzerland.

Wetter, Michael. 2011. "Co-Simulation of Building Energy and Control Systems with the Building Controls Virtual Test Bed." *Journal of Building Performance Simulation* 4 (3): 182–203. https://doi.org/10.1080/19401493.2010.518631.

Wetter, Michael, Wangda Zuo, Thierry S. Nouidui, and Xiufeng Pang. 2014. "Modelica Buildings Library." *Journal of Building Performance Simulation* 7 (4): 253–270. https://doi.org/10.1080/19401493.2013.765506.

Wienold, Jan, Francesco Frontini, Sebastian Herkel, and Sandra Mende. 2011. "Climate Based Simulation of Different Shading Device Systems for Comfort and Energy Demand." In *12th Conference of International Building Performance Simulation Association*. Sydney, Australia.

Zhao, Wanfang, Wei He, Zhongting Hu, Xiaoyu Zheng, Sheng Zhang, Gaofei Xu, Hongbing Chen, and Yanping Yuan. 2022. "Daylight and Thermal Performance of a Switchable Ethylene Tetra-Fluoro-ethylene Cushion with Dynamic Control in Different Climates." *Building Simulation* 15 (1): 29–40. https://doi.org/10.1007/s12273-021-0794-7.

Appendices

Appendix 1. Literature review

Table A1. Literature review on coupling and control of complex light dynamics. Column identifiers according to Table A2.

		CLDM model											Total model					
Ref	Type	str	tec	metV	metS	toolV	toolS	nu	nDis	query	ipol	sup	str	tec	toolCP	toolT	toolC	typeC
Gehbauer, Lee, and Wang (2023)	tint state	seq	o2o	3pm	3pm	R	R	3	4	dis	–	yes	biDT	o2o	Py	Mo	Py	hr, ob
Gehbauer et al. (2020)		seq	o2o	3pm	3pm	R	R	3	4	dis, con	yes	yes	biDT	o2o	Py	Mo	Py	hr, ob
Ganji Kheybari et al. (2021)		seq	o2o	3pm	–	R, W	W	3	2	con	yes	no	biDT	miw	BB	TS	Ma	hr, ob
Shen and Han (2022)	rot. angle	seq	o2o	2pm	–	R	–	45	11	dis	–	yes	biD	o2o	Py	–	Py	ob
Tabadkani et al. (2022)		?	o2o	?	–	?	–	3	4	dis	–	no	biD	o2o	Py	–	Py	hr
Coffey et al. (2022)		seq	o2o	3pm	3pm	R	R	2	11	dis	–	yes	biDT	o2o	Py	Mo	Py	ob
de Vries, Loonen, and Hensen (2021)		seq	o2o	3pm	KM	R	W	1	24	dis	–	–	biDT	miw	BB	E+	Ma	hr
Vlachokostas and Madamopoulos (2017)		seq	o2o	5pm	KM	R	W	1	13	dis	–	–	biD	o2o	–	E+	?	hr
Bueno, Cejudo-Lopez, and Kuhn (2017)		seq	o2o	–	KU	–	KU	1	2	dis	–	–	biT	o2o	Fe	Fe	Fe	hr
Bueno et al. (2015)		seq	o2o	3pm	KM	R	R	2	4/3	dis	–	?	biDT	o2o	Fe	Fe	Fe	hr
Vera et al. (2016)		seq	o2o	3pm	–	R	–	1	2	dis	–	–	biD	o2o	C	E+	C	hr
Molina (2014)		seq	o2o	3pm	KM	R	W	1	6	dis	–	–	biD	o2o	C	E+	C	hr
Wienold et al. (2011)		seq	o2o	?	KU	R	KU	1	18	dis	–	–	biD	o2o	?	Er	?	hr
Carlucci et al. (2023)	height	seq	o2o	?	?	E+	E+	1	3	dis	–	–	seq	o2o	Py	E+	Py	hr
Zhao et al. (2022)	gap width	?	o2o	?	–	R	–	1	2	dis	–	–	biD	miw	G	E+	G	hr
Weber et al. (2023b)		seq	o2o	–	KM	–	W	1	5	con	yes	–	biT	o2o	Mo	Mo	Mo	hr
Weber et al. (2023a)		seq	o2o	3pm	KM	R	W	1	5	con	yes	–	biDT	o2o	Mo	Mo	Mo	hr
t.w.		seq	si	3pm	KM	R	W	1	5	con	yes	–	biDT	o2o	Mo	Mo	Mo	hr

Table A2. Descriptions for Table A1.

Column identifier	Description of column identifier	Options	Description of option
type	Type of façade input		
str	Coupling strategy of either the CLDM or total model, cf. Taveres-Cachat et al. (2021)	seq	sequential
		biD	bidirectional on daylight states
		biDT	bidirectional on daylight and thermal states
		biT	bidirectional on thermal states
tec	Coupling technique of either the CLDM or total model, cf. Taveres-Cachat et al. (2021)	o2o	one-to-one
		miw	middleware
		si	standard interface
toolV	Tool to determine CLDM, visual domain	R: RADIANCE, W: WINDIW, KU: Kuhn method, Mo: Modelica, TS: TRNSYS, E+: EnergyPlus, Fe: Fener, Er: ESP-r, Py: Python, Ma: MATLAB, C: C, G: Grasshopper, BB: BCVTB	
toolS	Tool to determine CLDM, solar domain		
toolT	Tool for thermal dynamics		
toolC	Tool for control dynamics		
toolCP	Tool for coupling of the total model		
metV	Method to determine CLDM, visual domain	2pm, 3pm, 5pm: 2-, 3-, 5-phase method; KM: Klems-method / LBNL-Method; KU: Kuhn method	
metV	Method to determine CLDM, solar domain		
nu	Dimension of individual façade inputs		
nDis	Number of discretisation for each façade input		
query	CLDM query regarding the façade inputs	dis	discrete
		con	continuous
ipol	Interpolation between the discrete façade input points applied (only evaluated if query = con)	yes	
		no	
sup	Superposition method applied (only evaluated if nu > 1)	yes	Parallel SISO models plus superposition
		no	one MISO model cmp. Figure 2
typeC	Type of control	hr	heuristic based, i.e. threshold, P-control
		ob	optimization based (nlp, ip, mip)

Appendix 2. Hemispherical integral limits

This section presents the integration limits of the double integral, cf. Equation (12) for the three integration regions. Equations (A1) to (A4) hold for the entire range $\beta \in [0^\circ, 90^\circ]$, whereas Equations (A5) and (A6) are restricted to the two slopes $\beta = \{0^\circ, 90^\circ\}$. As in the thesis (Rüdisser 2023), a horizon band thickness of $b = 6.5^\circ$ was assumed.

$$\theta_{sky,lb} = 0 \tag{A1}$$

$$\theta_{sky,ub} = \begin{cases} \dfrac{\pi}{2} & \phi_w \leq \pi \\ \arctan\left(\dfrac{1}{\tan(\beta)\sin(\phi_w - \pi)}\right) & \text{else} \end{cases} \tag{A2}$$

$$\theta_{gnd,lb} = \theta_{sky,ub} \tag{A3}$$

$$\theta_{gnd,ub} = \frac{\pi}{2} \tag{A4}$$

$$\theta_{hor,lb} = \begin{cases} \dfrac{\pi}{2} - b & \beta = 0 \\ \begin{cases} 0 & \phi_w \leq \pi \\ \dfrac{\pi}{2} & \text{else} \end{cases} & \beta = \dfrac{\pi}{2} \end{cases} \tag{A5}$$

$$\theta_{hor,ub} = \begin{cases} \dfrac{\pi}{2} & \beta = 0 \\ \begin{cases} \arccos\left(\sqrt{\dfrac{1 - \cos\left(\frac{\pi}{2} - b\right)^2}{\left(1 + \frac{1}{\tan(\phi_w)^2}\right)}}\right) & \phi_w \in [b, \pi - b] \\ \dfrac{\pi}{2} & \text{else} \end{cases} & \beta = \dfrac{\pi}{2} \end{cases} \tag{A6}$$